Synthesis of RuO 2 nanowires from Ru thin films by atmospheric pressure micro-post-discharge

D. Kuete Saa, T. Gries, S. Migot-Choux, J. Ghanbaja, D. Mangin, P. Boulet, S. Laminsi, T. Belmonte

▶ **To cite this version:**

D. Kuete Saa, T. Gries, S. Migot-Choux, J. Ghanbaja, D. Mangin, et al.. Synthesis of RuO 2 nanowires from Ru thin films by atmospheric pressure micro-post-discharge. Surface and Coatings Technology, 2016, 295, pp.13-19. 10.1016/j.surfcoat.2015.12.005 . hal-02113600

HAL Id: hal-02113600
https://hal.science/hal-02113600

Submitted on 30 Apr 2019

HAL is a multi-disciplinary open access archive for the deposit and dissemination of scientific research documents, whether they are published or not. The documents may come from teaching and research institutions in France or abroad, or from public or private research centers.

L'archive ouverte pluridisciplinaire **HAL**, est destinée au dépôt et à la diffusion de documents scientifiques de niveau recherche, publiés ou non, émanant des établissements d'enseignement et de recherche français ou étrangers, des laboratoires publics ou privés.

Synthesis of RuO_2 nanowires from Ru thin films by atmospheric pressure micro-post-discharge

D. Kuete Saa[1,3], T. Gries[2], S. Migot-Choux[2], J. Ghanbaja[1], D. Mangin[1], P. Boulet[2], S. Laminsi[3], T. Belmonte[2,*]

[1]Université de Lorraine, UMR CNRS 7198, Institut Jean Lamour – Département Chimie et Physique des Solides et des Surfaces, Parc de Saurupt – CS 50840, F-54011 Nancy cedex France

[2]CNRS, Institut Jean Lamour, UMR CNRS 7198, NANCY, F-54042, France

[3]Université de Yaoundé 1, Laboratoire de Chimie Physique et Analytique Appliquées, 812 Yaoundé, Cameroun

*Corresponding author: Tel.: +33 383 584 251

thierry.belmonte@univ-lorraine.fr

Keywords: Ruthenium oxide; Nanowires; plasma process.

Abstract

Oxidation by a micro-post-discharge at atmospheric pressure of thin films of ruthenium deposited on fused silica by pressure-modulated magnetron sputtering is studied. Single-crystalline RuO_2 nanowires are obtained for the first time with a diffusion process over large areas. Nanowires grow typically at temperatures below 550-600 K, provided the level of stress is high enough to fragment grains in sub-grains with sizes between 30 and 50 nm. Because of the alternation of dense and porous layers forming the coating, inward diffusion of vacancies leads to no patent Kirkendall's effect, pores being distributed over the whole coating thickness and not mainly at the interface with the substrate. The centre of the treatment being heated at temperatures higher than 900 K, gaseous RuO_4 is formed, leading to an evaporated area. At its edge, a ring of microcrystals is formed, likely by a CVD mechanism.

1. Introduction

RuO_2 is an attractive electrical material because its room-temperature resistivity is 35 μΩ cm, *i.e.* about twice that of metallic Ru. It crystallizes in the rutile structure. Nanowires of RuO_2 had been produced by using templates [1], chemical vapour deposition [2] or reactive sputtering [3]. They can be used as interconnects in electronic applications [4] or electrochemical capacitors [5].

If high quality growth of RuO_2 nanowires has been reported [6-8], growing large areas by simple thermal heating of ruthenium is not possible, unlike what is observed with copper [9, 10] or iron [11, 12]. This is due to passivation properties of RuO_2. A dense oxide layer stops diffusion at low temperature. To enhance it, temperature must be increased. Then, anisotropic diffusion, which is a mandatory requirement for the synthesis of nanostructures, is hindered and the passive layer evenly increases in thickness. In a former work [13], the growth of localised concentric rings of RuO_2 nanowires was made possible on ruthenium substrates by resorting to post-discharge treatments operating at lower temperature than thermal heating. The presence of oxygen atoms and excited states of O_2 like the singlet state $O_2(a^1\Delta_g)$ in the spatial micro-post-discharge of a microwave plasma [14] enhances oxidation rates, which consequently allows a temperature decrease of about 100 K. With such a decrease, it is possible to grow a general nanostructure, made of RuO_2 lamellae separated by 20–50 nm and localised concentric rings of RuO_2 nanowires (figure 3 in ref. [13]) through emerging surface defects. The corresponding growth mechanism was already observed in the synthesis of localised concentric rings of silica nanowires on silicon wafers [15]. Then, two types of oxides have to be considered depending on whether they are passive or not.

In this work, we study the growth of nanostructures on ruthenium layers deposited on fused silica substrates and oxidised in a micro-post-discharge at atmospheric pressure. Thin films

affect the growth of nanostructures because of the change in the stress level that arises when a ceramic substrate is used instead of a metallic one that better accommodates strain.

2. Experimental setup

2.1. Oxidation process

The experimental set-up is shown in figure 1. The atmospheric microwave plasma is created in a fused silica tube (27 mm inner diameter) located in a 2.45 GHz resonant cavity. The power supply is a GMP 03 KE SAIREM device and it delivers 100W under the present conditions. Flow rates of gases are controlled by two mass flow controllers and the total flow rate is 413 sccm (standard cubic centimetre per minute). The partial pressure of oxygen in gas mixture (Ar-O_2) is 7.5 vol.%. The micro-afterglow flows through a hole (600 µm in diameter) made in the resonant cavity, forming a kind of beam [14]. This beam is mainly composed of O, $O_2(X)$, $O_2(a)$ and Ar species. No ozone is present because the gas is too hot (~ 1600 K at the nozzle exit). The sample-nozzle distance was set to 4.5 mm. The experimental conditions retained for this work are the best found to get the highest density of nanostructures, the influence of the main parameters (total flow rate, amount of oxygen, substrate nature and sample-nozzle distance) being not reported here.

Samples used are squares of fused silica (1.4×1.4×0.5 mm^3) coated by a 900 nm thick metallic ruthenium layer deposited by magnetron sputtering. The sputtering reactor is equipped with a pure (99.99 wt.%) ruthenium target. It is pumped down to 10^{-4} Pa, before being vented by an Ar-10vol.%H_2 mixture (total flow rate: 50 sccm). The total pressure is set at 0.58 Pa and the target-substrate distance is 10 cm. Before deposition, target and substrate are sputtered during 5 min at 80 W to clean surfaces. Deposition beyond typically 85 nm in thickness is not possible due to the development of an extremely high stress and the coating systematically peels off. Algoz *et al.* [16] studied the evolution of compressive stress during thin film deposition of ruthenium on silicon by magnetron sputtering. They showed that stress was

higher in dense layers deposited at low pressure (0.27 Pa) and lower at high pressure (2.7 Pa). By varying the pressure, they could deposit 2 µm thick Ru layers, relaxing the compressive stress by an alternation of porous and dense layers as shown by Karabacak *et al*. [17]. We applied their method and deposited stacks of 6 times 2 layers (one porous (70 nm at 2.3 Pa) and one dense (80 nm at 0.60 Pa)) to get a 900 nm thick coating (**supporting material 1**). Radial homogeneity is ensured by rotating the substrate-holder at a constant speed of 26 round min^{-1}.

By changing the treatment time, different oxide nano-objects could be grown and were characterised by several surface diagnostics. Scanning Electron Microscopy (SEM) was made with a Philips XL 30. A CAMECA IMS 7F instrument was used for Secondary Ion Mass Spectrometry (SIMS). A Cs^+ primary ion beam of 30 nA operating at 5 kV was used to sputter sample with an impact energy of 3 keV. Mass Resolving Power was set to 2000. Depth-profiles were acquired over an area of 100×100 μm^2. X-ray Diffraction using Co-Kα radiation (λ = 0.179026 nm) was performed with a Bruker D8 Discover diffractometer . To perform localised analyzes, θ/θ measurement with the parallel beam geometry and using a beam collimator of 300 µm as a diameter was used.. In this configuration, the analysed area is limited to a maximum of 300 µm×1mm in the 2-theta range scanned and the depth of the sample probed by X-rays is estimated to 1 to 3 µm. Transmission electron microscopy (TEM) investigation was performed on as-grown nano-objects with a JEOL ARM 200F – Cold FEG TEM/STEM running at 200 kV (point resolution 0.19 nm) fitted with a GIF Quatum ER.

2.2. Surface temperature

Surface temperature has a key role in the growth of nanostructures. In the specific case of ruthenium, oxidation of RuO_2 above 900 K precisely leads to the formation of a RuO_4 vapour [18]. Then, no nanostructure can be formed in these conditions, the oxide layer being evaporated. This phenomenon leads to the etching of the substrate. When the temperature

decays radially below 900 K, evaporation stops and nanostructures can be formed. Between the two areas, a pretty sharp interface appears. This is clearly visible (See **supporting material 2**). The radius of the evaporated area is easily determined geometrically. It evolves as the square root of time because it is limited by the formation of Kirkendall's porosity, a diffusion-controlled process, as discussed hereafter.

A transient heat transfer model, developed in a former work of ours (see reference [15] for a complete description of the model) was used to estimate the surface temperature. A 0.5 mm-thick cylindrical substrate (14 mm in diameter) made of fused silica and covered by a 900 nm-thick Ru layer was modelled. The temperature distribution in the micro-afterglow was determined from the OH ($A^2\Sigma^+$; $v' = 0 - X^2\Pi$; $v'' = 0$) rotational spectrum recorded at 306.4 nm by optical emission spectroscopy with an iCCD camera (see [15] for details). The maximum value was found to be 1600 K.

The calculated temperature gradient along the sample surface is given in figure 2. At steady state, which is reached theoretically after a couple of minutes typically, the maximum temperature is slightly below 900 K. This value is in good agreement with experimental results. In our experimental conditions, the value 900 K is reached 700 µm away from the treatment centre after 30 min.

The difference in the temperature profiles is attributed to the development of pores throughout the coating and not at the interface with the fused silica substrate, contrary to what is normally encountered with Kirkendall's porosity (see discussion). It contributes to create a porous material with lower thermal conductivity over its whole thickness and not mainly at the interface with the substrate. Although long nanowires are present above the coating, proving a strong mass transport outward, no large cavities or pores – as they are commonly observed in copper oxidation (see *e.g.* [10]) – are visible at the interface with fused silica. Here, the coating is rather dense even though a significant change in density can be noticed all

over the thickness with respect to the untreated coating (**see supporting material 1**). Indeed, the growth of the ruthenium oxide layer is due to outward diffusion of ruthenium ions as described in reference [13] and inward diffusion of vacancies which aggregate and form pores. The specificity of this mechanism in the present case comes from the density modulations induced by the coating process. The sputtered Ru coating is made of an alternation of more or less dense layers. Vacancies are likely trapped during their transport toward the substrate in layers of higher density and do not cross the whole coating. This question will be discussed further below (see SIMS results hereinafter). Anyway, the thermal conductivity decreases as porosity develops.

To account for this phenomenon in the model, the thermal conductivity of the layer was multiplied by a coefficient α lower than 1. If $\alpha = 0.57$, a perfect match is obtained with the experimental result (figure 2). The maximum temperature is then slightly higher (~1000 K). So, the simple approach used here helps us to determine approximatively how the modification of the thermal conductivity affects the temperature profile versus time.

3. Results and discussion

In the chosen experimental conditions, three types of RuO_2 objects are formed (figure 3). From the centre outward, one finds microcrystals, nanowires and nanodots. Microcrystals, with mean sizes of the order of a few micrometres, are assembly of faceted crystals which seem to interpenetrate and share common faces. Nanowires are also faceted and not cylindrical. Microcrystals are located at the edge of the evaporated area and form a kind of belt (Figure 4) where their average size increases outwards (**see supporting material 3**). This size gradient is all the more visible as treatment time is long. In the nanodot area, in the case of a 4-hour treatment, some large isolated microcrystals are also observed. Then, although transitions between the evaporated area and the microcrystals on the one hand, and between the microcrystals and the nanodots on the other hand, may defined by sharp edges (over 5-10

µm), they actually occur over hundreds of micrometers, *i.e.* quite smoothly. Nanodots are likely seeds of nanowires, but this is only a conjecture, this assertion remaining unproved. Then, we chose to distinguish these two latter nanostructures. The transition from nanowires to nanodots is mainly based on a subjective criterion defined by the possibility to measure a nanowire length (practically, beyond 50 nm) in top and cross-section views of SEM images. The transition from microcrystals to nanowires does not exhibit any sharp edge but it is progressive, isolated microcrystals being sometimes visible among the nanowires (unreported data).

From there on, a map showing the sharp transitions between the different RuO_2 objects could be drawn (figure 5). When the treatment time is 30 min, microcrystals are obtained between +1000 µm and +2200 µm and nanowires in their early stages appear between +3800 µm from the treatment centre and +5000 µm. When the processing time is increased to 3 and 4 hours, microcrystals are shifted beyond +2300 µm and +2600 µm, respectively. However, the radial distance over which microcrystals are formed is roughly constant. Their growth is necessarily related to the evaporation of the central area. Unlike short treatment times, *i.e.* less than 2 hours, no nanowire is observed. Nanodots are found instead.

The domain where RuO_2 nanowires are formed is limited in the chosen experimental conditions. However, for treatment times shorter than 2 hours, nanowires are not localised on concentric rings, like in the case of ruthenium substrates [13], but spread over wide area. The non-localised production of RuO_2 nanowires is then possible, as shown in figure 6. We observe successive magnifications of homogeneously-coated area of about 10^4 μm^2 areas where nanowires with similar features are randomly distributed. Because of the temperature gradient prevailing radially, nanowires have not got the same features all over their existence domain. Their different characteristics (average length, average diameter and surface number density) were determined as a function of the radial distance between +2500 µm and +5500

for a 2-hour treatment (see **supporting material 4**). If the length and diameter of nanowires are maximal at +2500-3000 µm and decay farther, their density is twice higher at +5000-5400 µm. The minimum average diameter found in this study is about 50 nm, which is quite large. To conclude, there is an optimal oxidation time to synthesize nanowires. Beyond, nanowires disappear in favour of nanodots. This transformation is due to a burying mechanism described by [19]. Nanowires stop growing because of a change in the growth conditions (like a temperature rise) whereas the oxide layer develops outward, filling the space between nanowires and thus burying them.

In figure 7, X-ray diffraction patterns recorded after treatment at different radial positions are depicted. From outside inward, several aspects deserve serious examination. At +5.5 mm from the center, the diffraction peaks $(10\bar{1}1)$ and $(10\bar{1}0)$ of ruthenium are clearly observed. The (101) peak of ruthenium dioxide (RuO_2–tetragonal phase) is observed. This phase is the only oxide phase identified in this work. The (101) peak gradually increases when the analysed area is closer to the centre. A small additional peak at $2\theta = 64.29°$ appears at 4.5 mm. It corresponds to RuO_2 (211). The sample is more oxidised and the ratio between oxide and metal volumes probed by the X-rays increases. At 3.5 mm, the RuO_2 (101) peak has almost got the same intensity as the Ru $(10\bar{1}1)$ peak. A new peak is visible at $2\theta = 33°$. It is due to the RuO_2 (110). At 2.5 mm, the intensities of ruthenium peaks decrease whereas those of RuO_2 peaks increase. At this spot, the probed volume is mainly that of the RuO_2 layer. Finally, at 1.5 mm (*i.e.* about 200 µm from the evaporated area), the intensities of the ruthenium peaks are weak, showing a strong oxidation process.

High-resolution TEM analyses (see **supporting material 5**) show that nanowires are single-crystals. Micro-diffraction patterns always indicate the crystalline structure of tetragonal RuO_2 [20] but with various zone axes: the growth of single-crystalline nanowires occurs with random crystallographic orientations.

Radial and depth compositions of oxide layers were analysed by SIMS (figure 8). Usually, this type of analysis is not suitable for nanostructured thin films because of the effect that the morphology produces on the detected signal, the top of the nanostructures and the underlying layer being sputtered simultaneously. Let's mention first that no measurement was possible in the evaporated area. There, the ruthenium coating is almost totally removed by evaporation. The insulating properties of the uncoated fused silica hinder SIMS measurements.

To each depth-profile is assigned a SEM micrograph taken at the very spot where measurement was made. Results show that the oxidized sample is composed of ruthenium and oxygen with oscillating compositions due to the deposition process by magnetron sputtering. When ruthenium is high, the layer is more "metallic" and less porous. In figure 8, we clearly observe that oscillations are all the more damped, especially near the substrate, as nanowires are denser. They are also all the more overlapped. When the density is the highest (+3500 µm), the depth-profile is strongly perturbed and difficult to analyse, but all in all, the trend is clear. At the boundary with the nanodots (+5900 µm), the SIMS profile is almost identical to that of the non-treated coating.

The damping of the SIMS signals shows a higher homogeneity of Ru and O over the thickness. As expected, initially denser layers get more porous and the porosity is distributed over the whole coating, even though pores tend to accumulate at the inner interface, leading to a slightly negative slope of the element distribution inward. The formation of holes all along the thickness of the layer is clearly visible in figure 9. As diffusion occurs along grain boundaries, these holes are mainly localized along the layer columns. These data confirm the possibility of a specific behaviour of vacancies in a pressure-modulated coating.

During the first step of magnetron sputtering, stress in the deposited Ru film on fused silica could be mitigated by alternating low and high pressures deposition phases. Here, the main contribution to the development of stress is clearly related to the choice of the substrate. The

small difference in thermal expansion coefficients between Ru (6.4×10^{-6} K^{-1}) and RuO_2 (5.2×10^{-6} K^{-1}) induces the occurrence of a very weak compressive stress during oxidation, the growth of nanowires being not possible over large areas. Conversely, the huge difference in thermal expansion coefficients between fused silica (0.5×10^{-6} K^{-1}) and Ru and even RuO_2 contributes to create a high level of stress. Indeed, when the RuO_2 / Ru / substrate stack is heated, a differential expansion mainly between RuO_2 / Ru and SiO_2 occurs. The RuO_2 / Ru coating undergoes a compressive stress which leads to fragmentation of grains in sub-grains with mean size as low as 30-50 nm (figure 9). This mechanism generates defects in large quantities and enhances the outward transport of ruthenium by diffusion. The subsequent growth of long nanowires with high densities is thus made possible. The growth of RuO_2 nanowires on thin films would be akin to that of CuO on copper for example [19, 21], provided a sufficiently high level of stress is reached. The barrier effect caused by the passive nature of RuO_2 is suppressed by the strong fragmentation process resulting from the development of strain.

After a two-hour treatment, nanowires are found between 2.1 mm and 6 mm. They do not grow in the hotter area where microcrystals are observed. There, the temperature is too high to enable an anisotropic growth of the nanostructures. According to the results of our thermal model, the critical temperature beyond which nanowires stop forming is about 550-600 K (~ 300 ° C).

Concerning the mechanistic aspects of the RuO_2 nanowire growth, Coloma Ribera *et al.* [22], showed the existence of a low density RuO_x ($2 < x \leq 3$) layer limited to a maximum of 3 nm and located on top of a higher density stoichiometric RuO_2. This latter layer acting as a barrier, outward diffusion of ruthenium atoms becomes limiting, leading to synthesis of the oxygen-rich RuO_x upper layer. Up to a certain thickness, the oxide film remains quasi-amorphous to keep the minimum energy interface with ruthenium. At about 473 K, because of

the rather high mobility of Ru or Ru-O precursors at the surface, the first crystalline RuO_2 nuclei form at the topmost surface. Because the RuO_x is a rather disordered structure, it does not support 2D growth over large areas and RuO_2 crystallites continue to grow vertically. These authors observed the first crystalline columns near 550 K, which is the lower limit found of the temperature range found in our conditions. The outward diffusion of ruthenium predicted by this growth model is necessarily associated with the formation of pores in the layer. In the present case, because of the existence of a stack of bilayers with two different densities, the way the porosity is distributed in the oxidized layer is different from the one expected for a homogeneous layer.

The formation of microcrystals comes under a completely different mechanism. If the distance from the centre of the treatment is set to, say, 1 mm, increasing the temperature makes microcrystals disappear (figure 5). They are formed in a temperature range spanning from 550 to 900 K. Above 900 K, they are converted into gaseous RuO_4 and removed from the spot where they stood. This mechanism is supported by the existence of a size gradient (**See supporting material 3**). The observation of these objects in cross-section is particularly informative (Figure 3). Indeed, microcrystals can reach sizes of several micrometres in height after only 30 minutes, while the underlying layer of ruthenium is about 700 nm. On the other hand, the density of microcrystals is much higher than that of the underlying layer. Such a change in a process controlled by outward diffusion is simply inconceivable because short circuits are essential for nanowire growth. Therefore, microcrystals are likely formed by a CVD mechanism from RuO_4 generated in the central area. The growth of these objects would then be driven by a Volmer-Weber mechanism. This would explain why the domain where microcrystals are found (~1.5 mm in width – see figure 5) does not depend on time.

4. Conclusion

Contrary to raw ruthenium substrates, thin films of ruthenium deposited on fused silica by pressure-modulated magnetron sputtering enable the growth of single-crystalline RuO_2 nanowires over large area by micro-post-discharge oxidation at atmospheric pressure. They grow typically at temperatures below 550-600 K, provided the level of stress is high enough to fragment grains in sub-grains with sizes between 30 and 50 nm. The role of the micro-afterglow is mainly to provide active oxygen species like O or $O_2(a)$, enabling a reduction of the processing temperature. Because of the alternation of dense and porous layers forming the coating, inward diffusion of vacancies leads to no patent Kirkendall's effect insofar as pores are distributed over the whole coating thickness and not mainly at the interface with fused silica. Near the centre of the treatment where gaseous RuO_4 is formed as soon as the temperature is higher than 900 K, a ring of microcrystals is formed, likely by a CVD mechanism.

Acknowledgements

The “Service de Coopération et d'Action Culturelle” of the French embassy in Cameroon is gratefully acknowledged for the PhD grant of D. Kuete Saa.

References

[1] B.C. Satishkumar, A. Govindaraj, M. Nath, C.N.R. Rao, Synthesis of metal oxide nanorods using carbon nanotubes as templates, J. Mater. Chem. 10 (2000) 2115–2119

[2] C.C. Chen, R.S. Chen, T.Y. Tsai, Y.S. Huang, D.S. Tsai, K.K. Tiong, The growth and characterization of well aligned RuO_2 nanorods on sapphire substrates, J. Phys.: Condens. Matter 16 (2004) 8475–8484

[3] K.W. Cheng, Y.T. Lin, C.Y. Chen, C.P. Hsiung, J.Y. Gan, J.W. Yeh, C.H. Hsieh, L.J. Chou, In situ epitaxial growth of TiO_2 on RuO_2 nanorods with reactive sputtering, Appl. Phys. Lett. 88 (2006) 043115

[4] Y.L. Liu, Z.Y. Wu, K.J. Lin, Jr.J. Huang, F.R. Chen, J.J. Kai, Y.H. Lin, W.B. Jian, J.J. Lin, Growth of single-crystalline RuO_2 nanowires with one-and two-nanocontact electrical characterizations, Appl. Phys. Lett. 90 (2007) 013105

[5] P. Chen, H. Chen, J. Qiu, C. Zhou, Inkjet printing of single-walled carbon nanotube/RuO_2 nanowire supercapacitors on cloth fabrics and flexible substrates, Nano Research 3 (2010) 594–603

[6] M. Kang, Y. Lee, H. Jung, J. H. Shim, N.-S. Lee, J. M. Baik, S. C. Lee, C. Lee, Y. Lee, M. H. Kim, Single carbon fiber decorated with RuO_2 nanorods as a highly electrocatalytic sensing element, Anal. Chem, 84 (2012) 9485–9491

[7] Y. Lee, B.-U. Ye, H. K. Yu, J.-L. Lee, M. H. Kim, J. M. Baik, Facile synthesis of single crystalline metallic RuO_2 nanowires and electromigration-induced transport properties, J. Phys. Chem. C, 115 (2011) 4611–4615

[8] S. Kim, Y. K. Cho, J. Seok, N.-S. Lee, B. Son, J. W. Lee, J. M. Baik, C. Lee, Y. Lee, M. H. Kim, Highly Branched RuO_2 Nanoneedles on Electrospun TiO_2 Nanofibers as an Efficient Electrocatalytic Platform, ACS Appl. Mater. Interfaces, 7 (2015) 15321–15330

[9] M. Chen, Y. Yue, Y. Ju, Growth of metal and metal oxide nanowires driven by the stress-induced migration, J. Appl. Phys. 111 (2012) 104305

[10] A. Altaweel, G. Filipič, T. Gries, T. Belmonte, Controlled growth of copper oxide nanostructures by atmospheric pressure micro-afterglow, J. Cryst. Growth 407 (2014)17–24

[11] D.A. Voss, E.P. Butler, and T.E. Mitchell, The growth of hematite blades during the high temperature oxidation of iron, Metall. Trans. A 13 (1982) 929–935

[12] N. Bertrand, C. Desgranges, D. Poquillon, M. C. Lafont, D. Monceau, Iron oxidation at low temperature (260–500 C) in air and the effect of water vapor, Oxid. Met. 73 (2010) 139–162

[13] D. Kuete Saa, R.P. Cardoso, F. Kosior, A. Al Taweel, T. Gries, S. Laminsi, T. Belmonte, Growth of ruthenium dioxide nanostructures by micro-afterglow oxidation at atmospheric pressure, Surf. Coat. Technol. 255 (2014) 3–7

[14] G. Arnoult, R. P. Cardoso, T. Belmonte, G. Henrion, Flow transition in a small scale microwave plasma jet at atmospheric pressure, Appl. Phys. Lett. 93 (2008) 191507

[15] G. Arnoult, T. Gries, G. Henrion, S. Migot, V. Fournée, T. Belmonte, Localized Growth of Silicon Oxide Nanowires by Micro-Afterglow Oxidation, Plasma Process. Polym. 9 (2012) 1125–1131

[16] A. S. Alagoz, J. -D. Kamminga, S. Yu. Grachev, T. -M. Lu, T. Karabacak, « Residual stress reduction in sputter deposited thin films by density modulation », MRS Fall Meeting Proceedings 1224 (2009) 1224-FF05-22

[17] T. Karabacak, C. R. Picu, J. J. Senkevich, G. -C. Wang, T. -M. Lu, Stress reduction in tungsten films using nanostructured compliant layers, J. Appl. Phys. 96 (2004) 5740–5746

[18] J. C. Chaston, Reactions of oxygen with the platinum metals, Platinum Met. Rev. 9 (1965) 126–129

[19] L. Yuan, Y. Wang, R. Mema, G. Zhou, Driving force and growth mechanism for spontaneous oxide nanowire formation during the thermal oxidation of metals, Acta Mater. 59 (2011) 2491–2425

[20] C.E. Boman, Refinement of the crystal structure of ruthenium dioxide, Acta Chem. Scand., 24 (1970) 116–122

[21] G. Filipič, U. Cvelbar, Copper oxide nanowires: a review of growth, Nanotechnol. 23 (2012) 194001

[22] R. Coloma Ribera, R. W. E. van de Kruijs, S. Kokke, E. Zoethout, A. E. Yakshin, F. Bijkerk, Surface and sub-surface thermal oxidation of thin ruthenium films, *Appl. Phys. Lett.* 105 (2014) 131601

FIGURE CAPTIONS

Figure 1: Experimental set-up.

Figure 2: Steady-state temperature profiles of the outermost surface of the sample for $\alpha=1$ and $\alpha=0.57$. Corresponding 2D-temperature distribution in colour map from model.

Figure 3: Top and cross-section views of the three nanostructures observed from the centre outward.

Figure 4: Detail of the microcrystals belt at the edge of the evaporated area after sufficiently long treatment time (4h in this example). In the nanodot area, some large isolated microcrystals are clearly visible.

Figure 5: Map showing the localization of nanostructures on the treated surface as a function of time.

Figure 6: Non-localised production of RuO_2 nanowires. Micrographs from a) to d) are successive magnification of squared areas. In micrograph a), nanowires coat homogeneously an area of about 10000 μm^2.

Figure 7: Radial evolution of X-ray diffraction patterns of a ruthenium film deposited on fused silica after a 2-hour treatment.

Figure 8: SIMS depth-profiles for different radial distances (treatment time: 2h). SEM micrographs correspond to areas where measurements were made.

Figure 9: SEM micrograph of nanowires synthesised after a processing time of 2 hours. An upper layer with lower grain size is distinctly visible. A zoom is provided where the transition between this layer and the one underneath is identified by a dotted line.

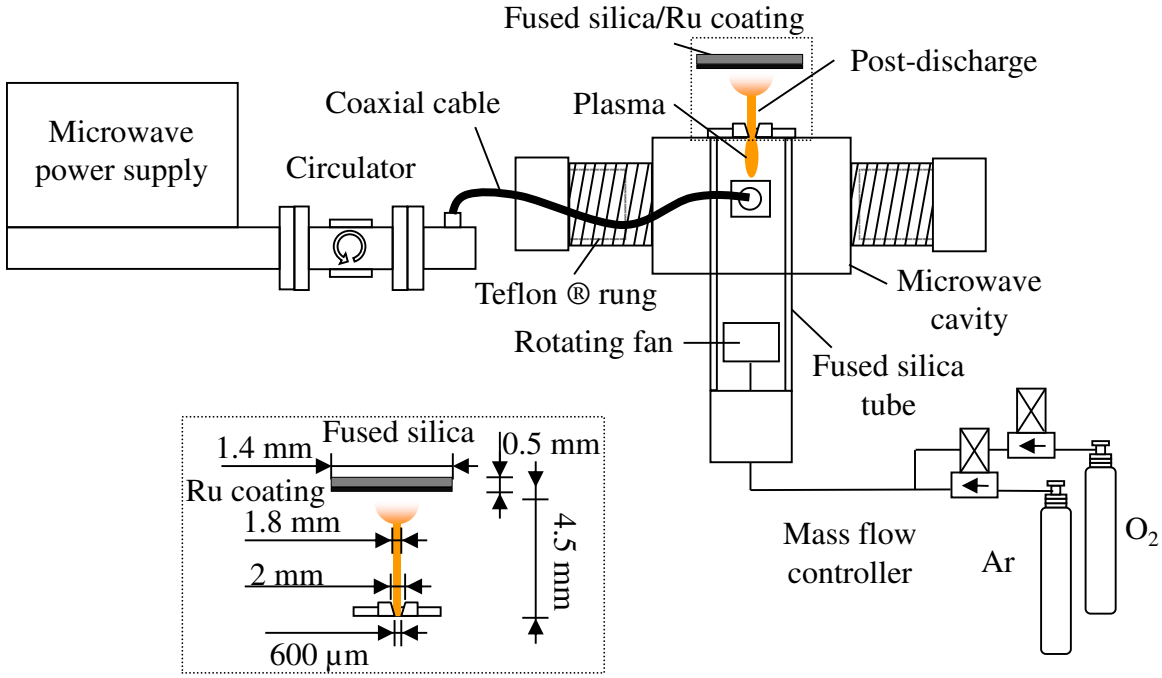

Figure 1: Experimental set-up.

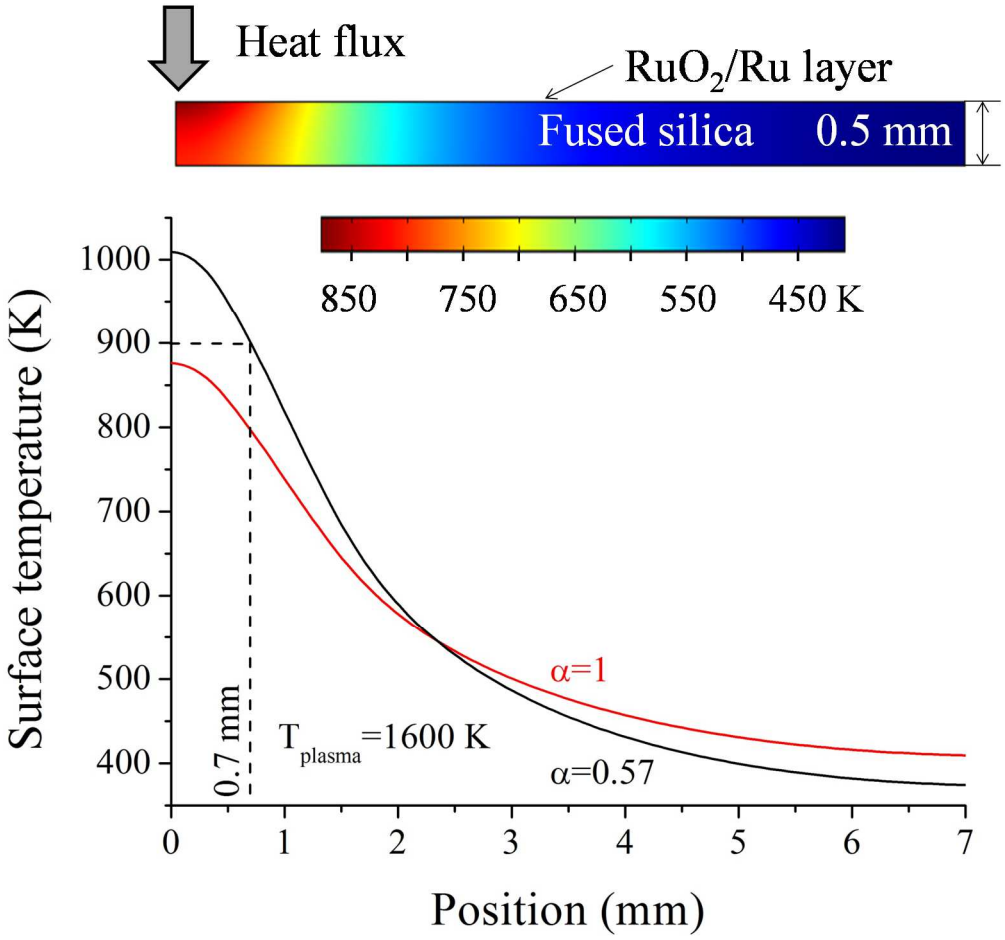

Figure 2: Steady-state temperature profiles of the outermost surface of the sample for α=1 and α=0.57. Corresponding 2D-temperature distribution in colour map from model.

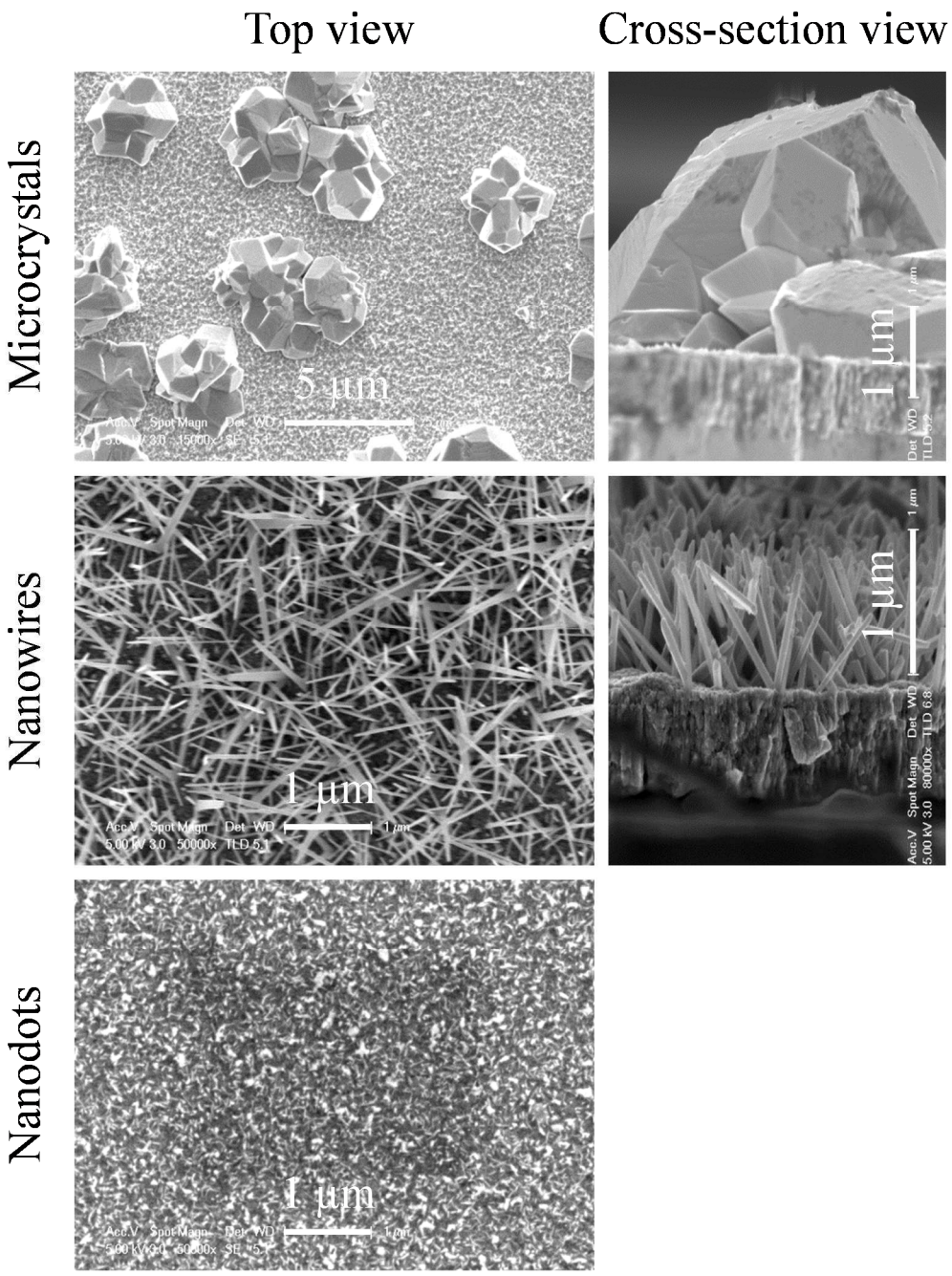

Figure 3: Top and cross-section views of the three main types of objects observed from the centre outward.

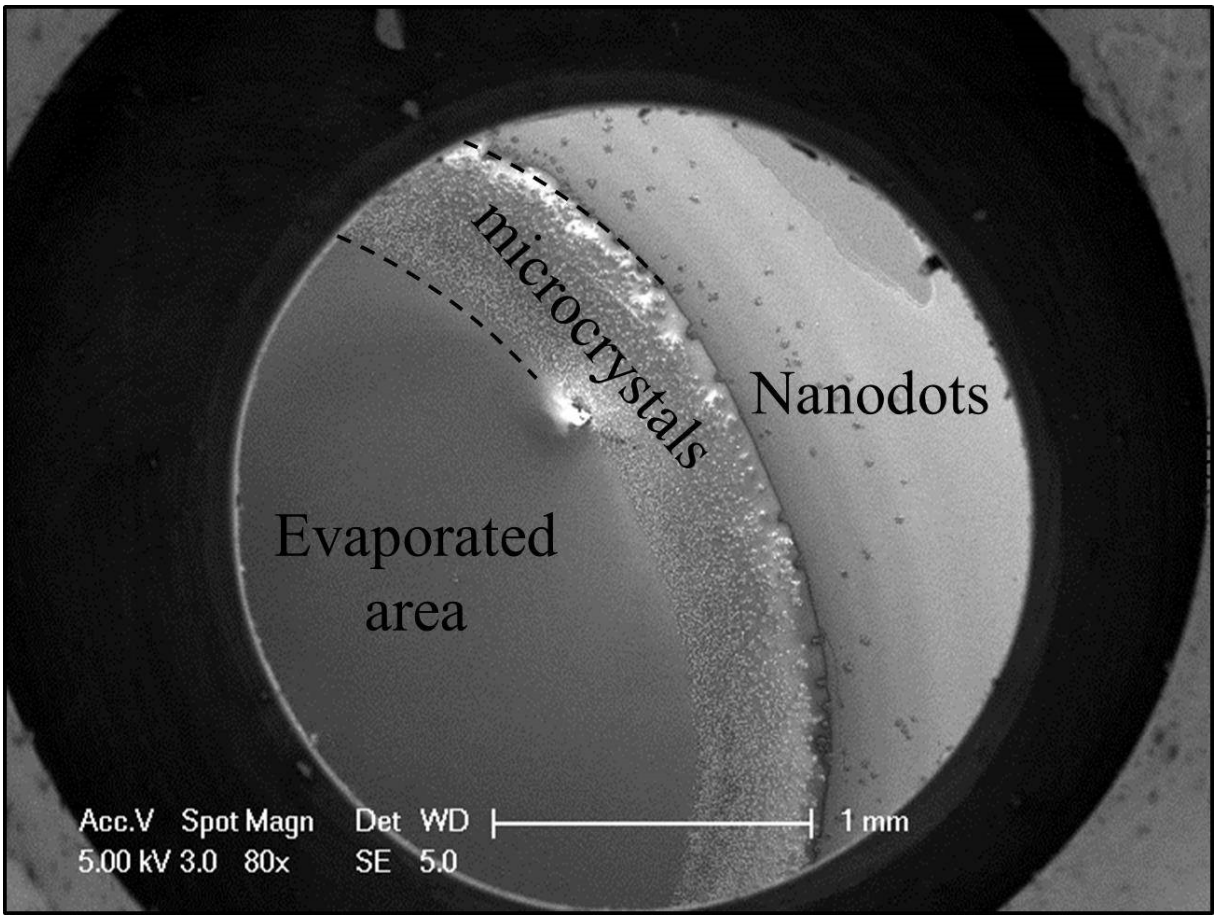

Figure 4: Detail of the microcrystals belt (shown by dashed lines) at the edge of the evaporated area after sufficiently long treatment time (4h in this example). In the nanodot area, some large isolated microcrystals are clearly visible.

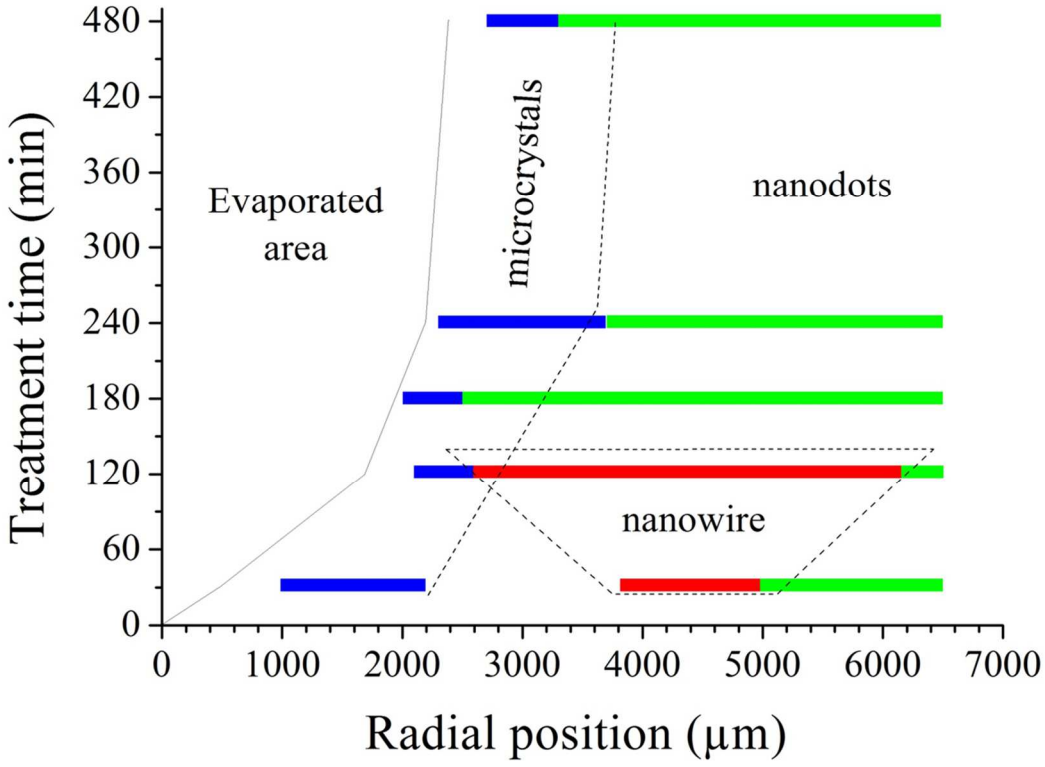

Figure 5: Map showing the localization of the three types of identified objects on the treated surface as a function of time.

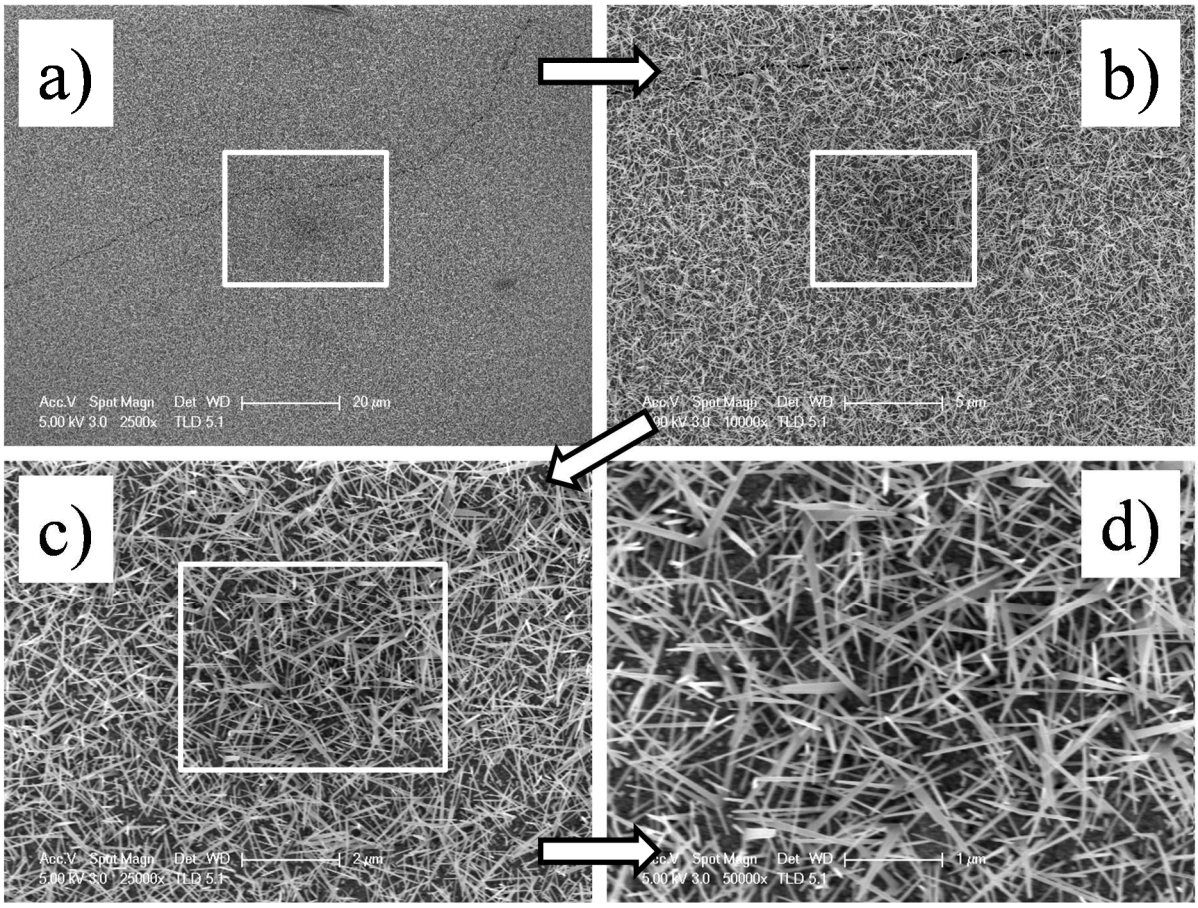

Figure 6: Non-localised production of RuO_2 nanowires. Micrographs from a) to d) are successive magnification of squared areas. In micrograph a), nanowires coat homogeneously an area of about 10^4 µm^2.

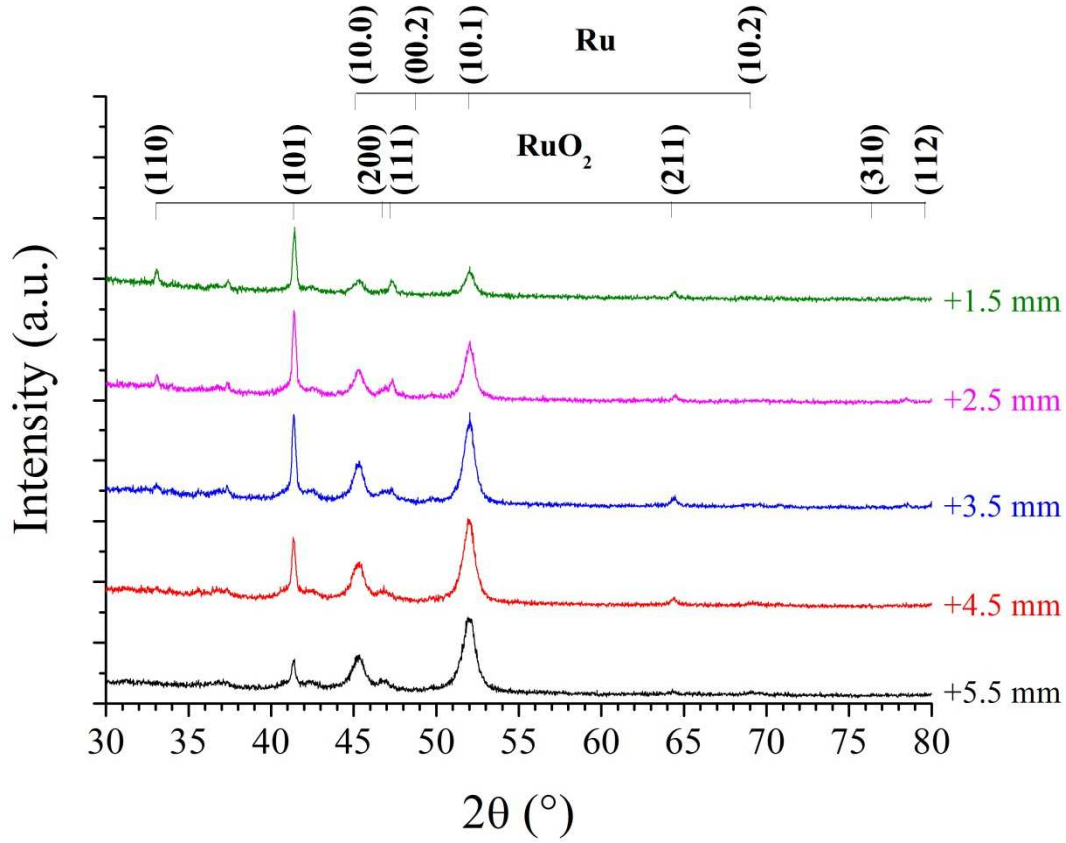

Figure 7: Radial evolution of X-ray diffraction patterns of a ruthenium film deposited on fused silica after a 2-hour treatment.

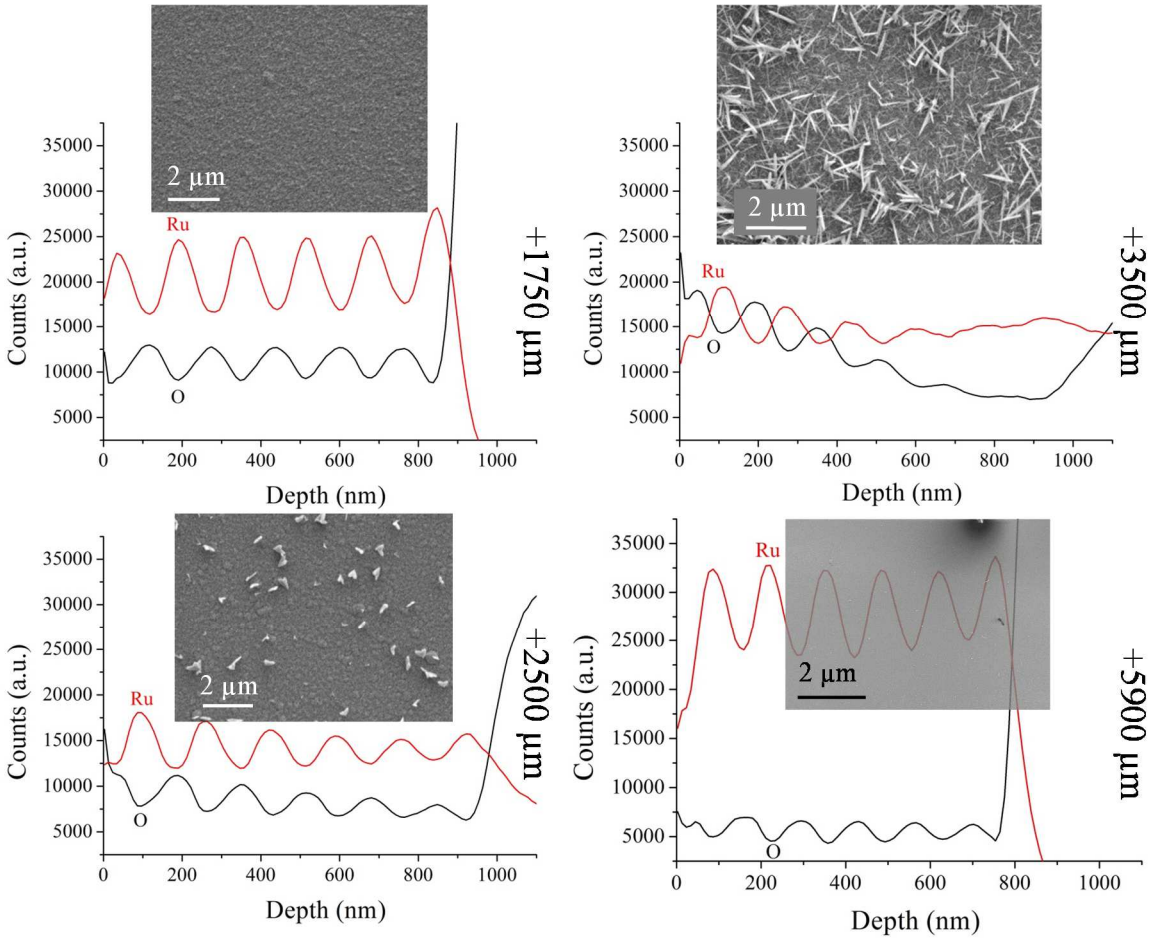

Figure 8: SIMS depth-profiles for different radial distances (treatment time: 2h). SEM micrographs correspond to areas where measurements were made.

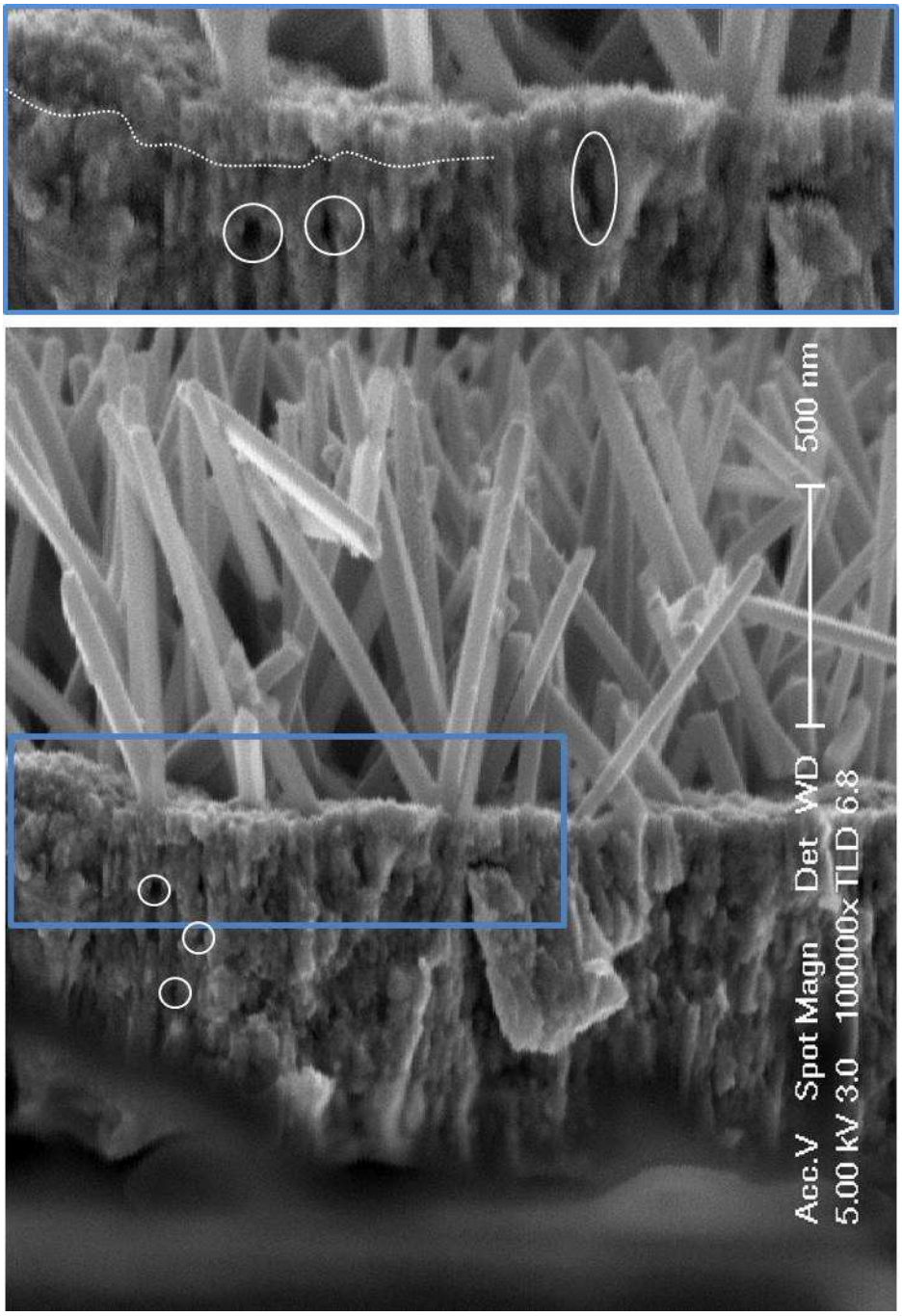

Figure 9: SEM micrograph of nanowires synthesised after a processing time of 2 hours. An upper layer with lower grain size is distinctly visible. A zoom is provided where the transition between this layer and the one underneath is identified by a dotted line. Circles indicate the presence of pores all over the layer thickness.

SUPPORTING MATERIALS FOR REFEREES

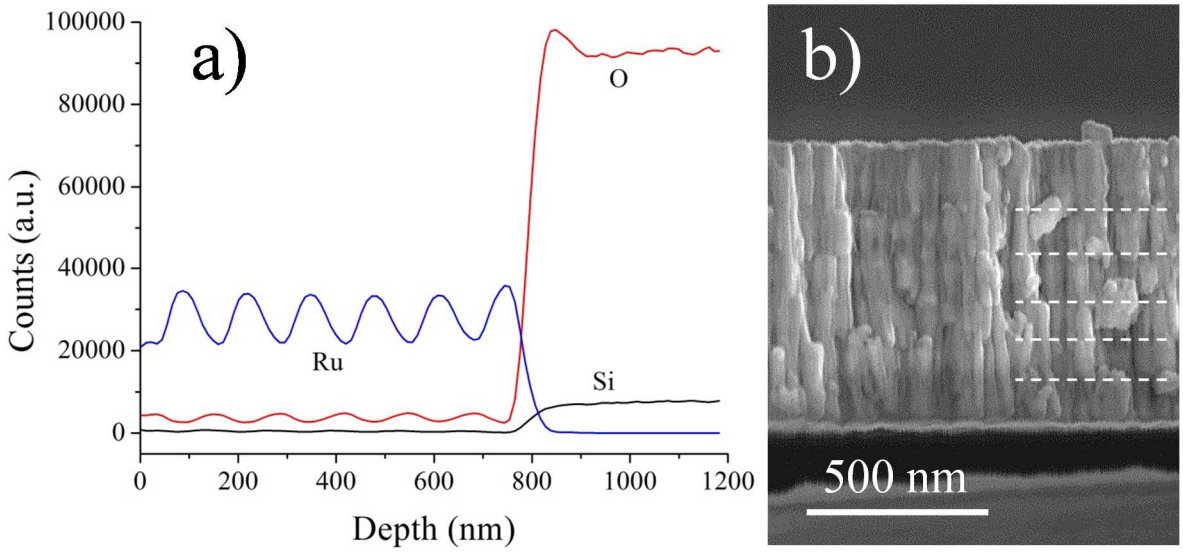

Supporting material 1: a) SIMS elements profile and b) corresponding SEM image of a ruthenium coating (thickness: ~900 nm) deposited by magnetron sputtering by applying a pressure modulation in time. Transitions between layers are visible in the SEM image and are materialised by dotted lines.

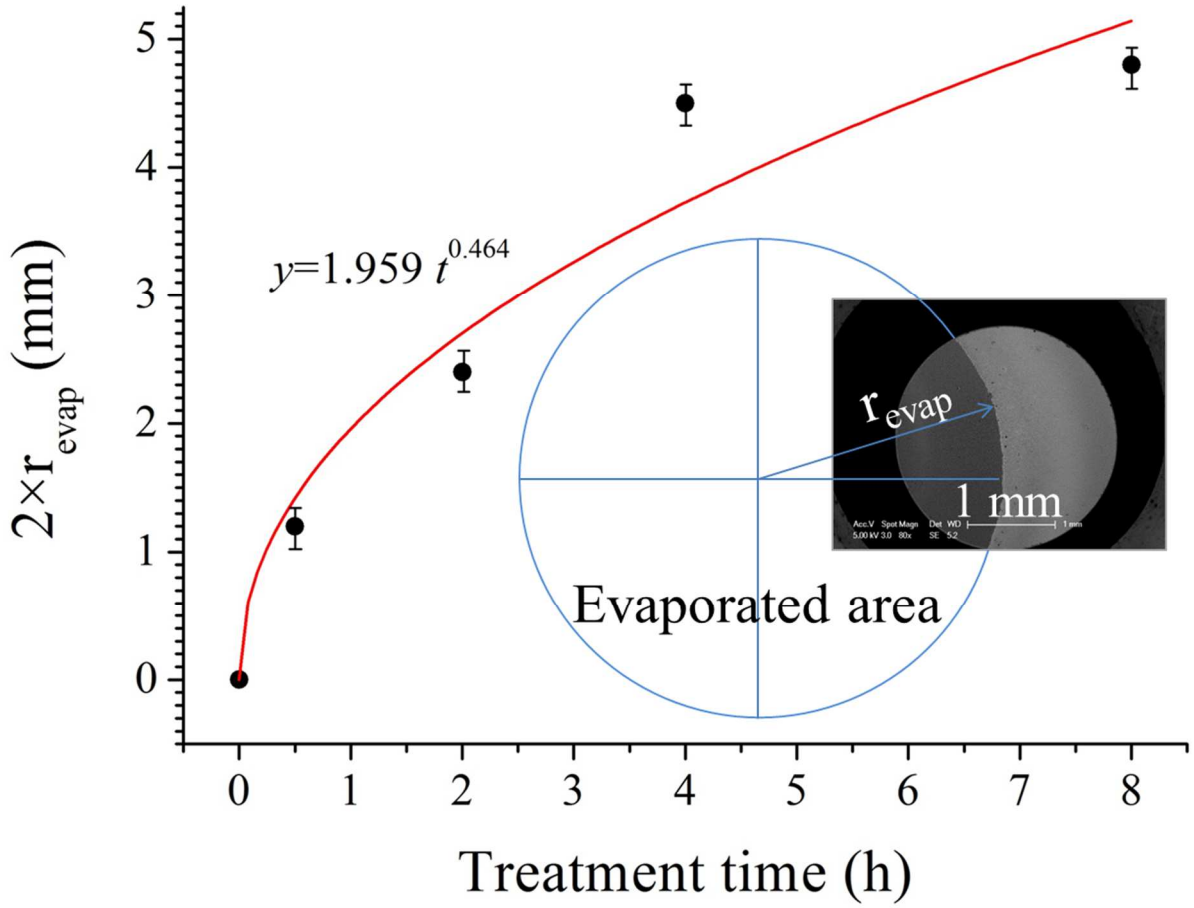

Supporting material 2: Time evolution of the diameter of the central area evaporated by the afterglow. The way the diameter is estimated is given by the inserted schematic where a SEM picture showing the transition between evaporated and coated areas is provided with the corresponding construction used to determine r_{evap}.

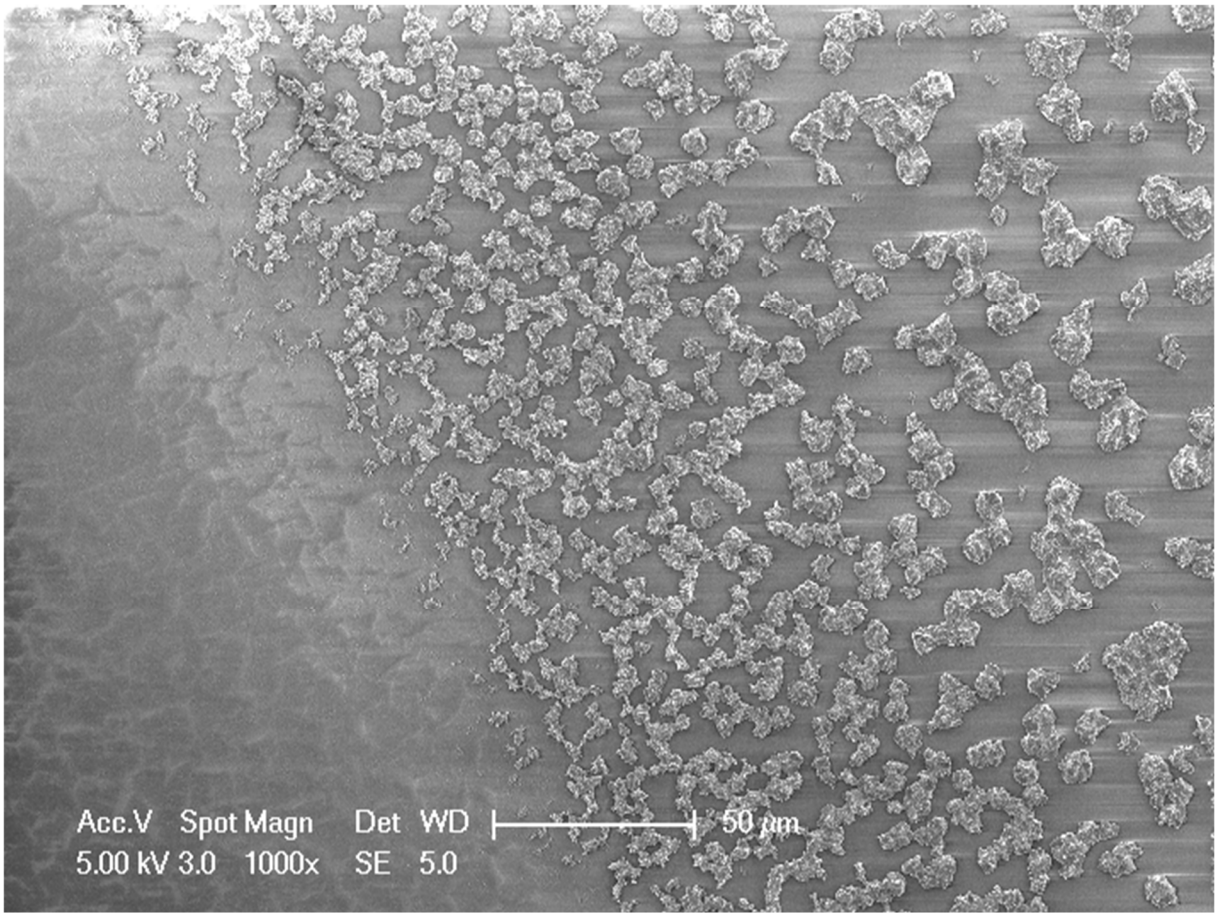

Supporting material 3: Magnification of the belt showing the microcrystal size gradient. This belt of microcrystals appears at the edge of the evaporated area after sufficiently long treatment time.

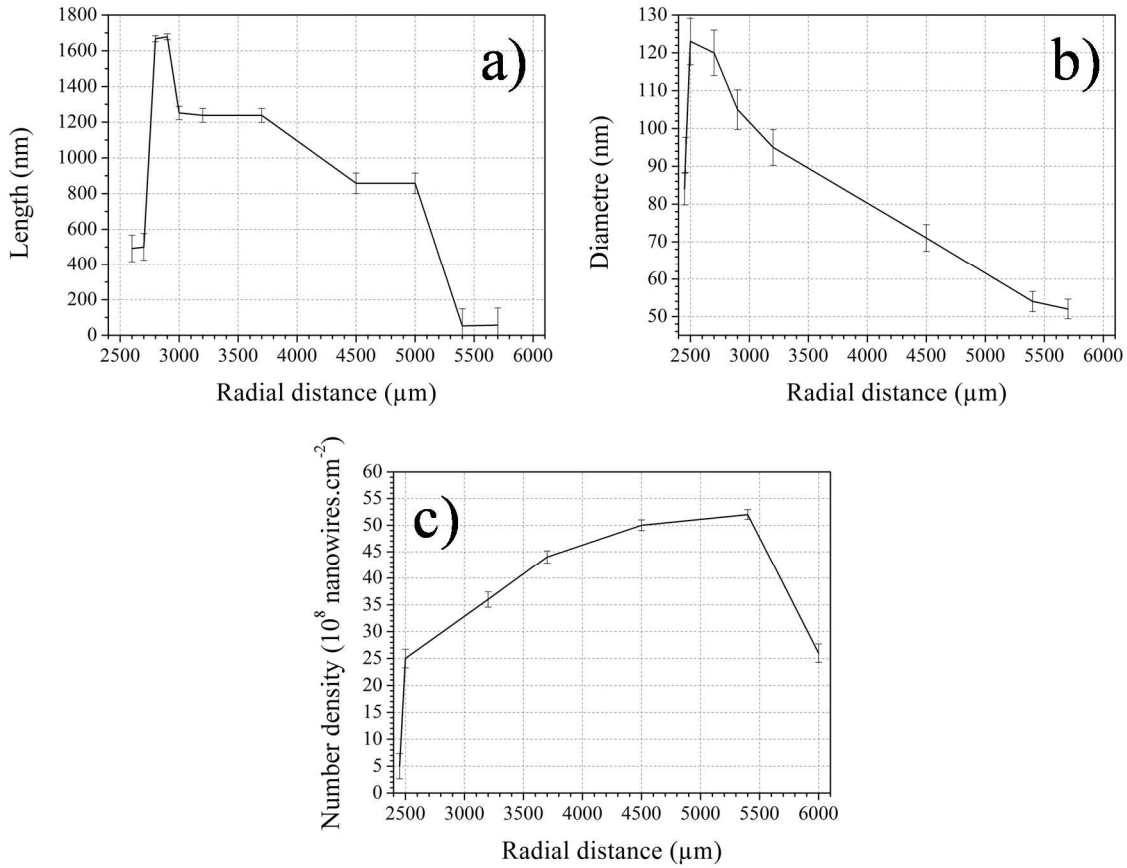

Supporting material 4: Evolutions of a) average length, b) average diameter and c) surface number density of nanowires as a function of the radial distance.

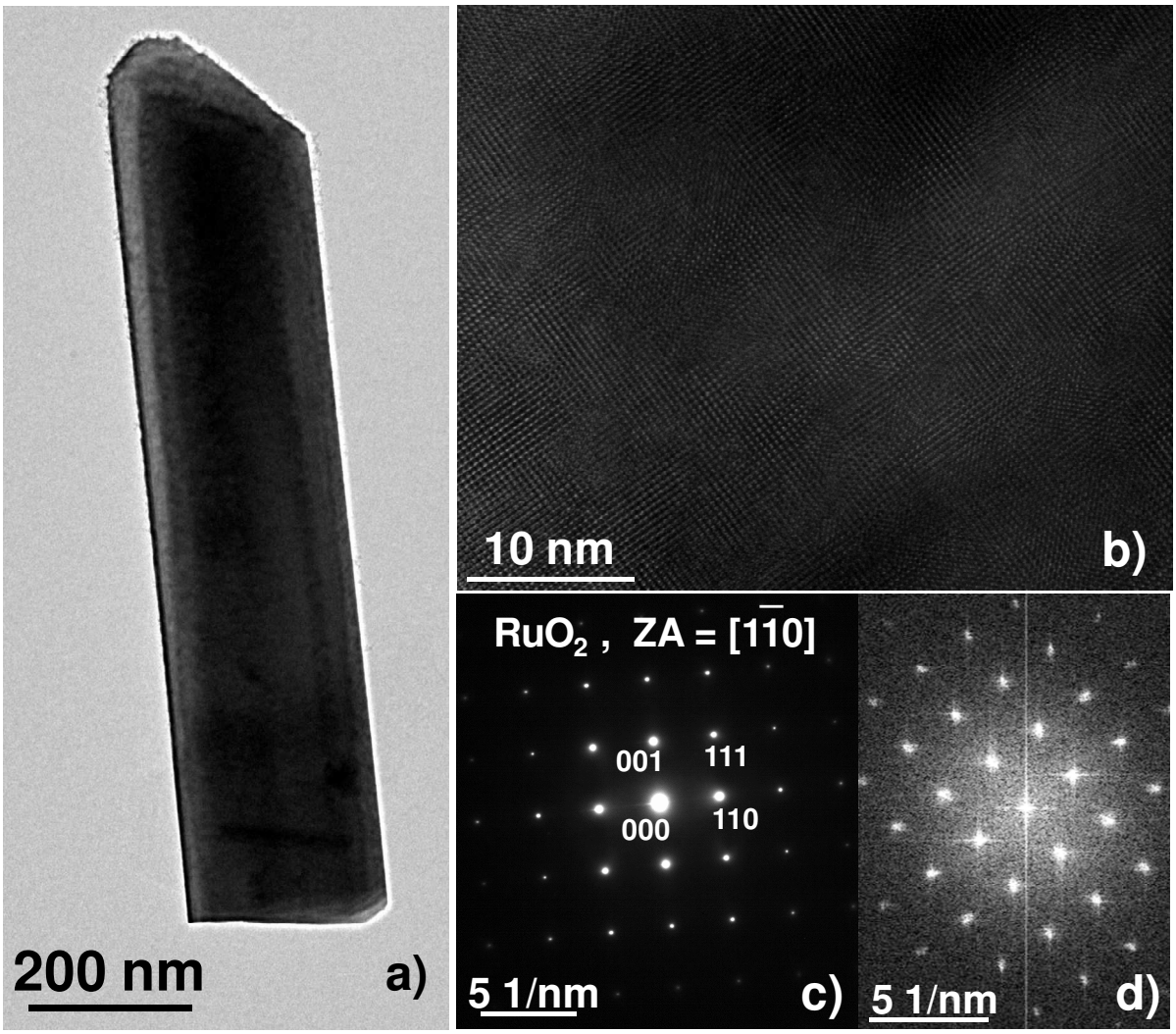

Supporting material 5: a) TEM Micrograph of a single-crystalline nanowire. b) high-resolution image of the selected nanowire. c) Micro-diffraction pattern of the nanowire appearing in the centre of figure a (ZA = zone axis). d) Fourier transform of figure b.

Nanowires are crystallized all over their diameter and length and no amorphous phase could be observed at edges. The spacing between adjacent planes is about 0.318 nm, which is consistent with the lattice parameter expected for the (110) plane of the tetragonal phase of RuO_2 (the theoretical value is 0.317 nm).